Appl Phys A (2009) 94: 775–780
DOI 10.1007/s00339-008-4957-5

Applied Physics A
Materials Science & Processing

The effect of pre-annealing of sputtered ZnO seed layers on growth of ZnO nanorods through a hydrothermal method

Shu-Yi Liu · Tao Chen · Jing Wan · Guo-Ping Ru · Bing-Zong Li · Xin-Ping Qu

Received: 18 August 2008 / Accepted: 20 October 2008 / Published online: 11 November 2008

Abstract Oriented ZnO nanorods were grown on ion-beam-sputtered ZnO seed layers through a hydrothermal approach without any metal catalyst. The sputtered ZnO seed layers were pre-annealed at different temperatures before the growth of ZnO nanorods. The effects of pre-annealing of the ZnO seed layers on the growth rate, crystallinity and optical properties of ZnO nanorods thereon were studied. The obtained ZnO nanorods had a wurtzite structure and grew along the preferential [0001] orientation with a normal direction to the substrates. Results show that the growth rate and density of the ZnO nanorods strongly depend on the pre-treatment conditions of the ZnO seed layer. With higher pre-treatment temperature, the crystallinity and surface characteristics of the ZnO seed layer were improved and thereafter the growth rate of ZnO nanorods thereon increased. Photoluminescence spectroscopy results show that the UV emission also becomes stronger and sharper with increasing annealing temperature of the ZnO seed layer.

PACS 61.46.Km · 81.16.Be · 81.40.Tv · 81.15.Jj · 81.40.Ef

1 Introduction

Zinc oxide (ZnO) has been widely studied because of its unique optical and electrical properties [1–4]. In recent years, nanoscale one-dimensional (1D) ZnO materials, i.e. nanorods or nanowires, have also received great interest due to their potential applications in electronic and optoelectronic devices [5], such as room-temperature ultraviolet lasers [6], solar cells [7], gas sensors [8], photodetectors [9], light-emitting diodes [10] and surface acoustic wave (SAW) devices [11]. Growth of functional ZnO nanomaterials with a highly aligned and oriented array takes an important role in the performance of these devices. Various methods have been used to fabricate aligned ZnO nanostructures, including metal–organic chemical vapor deposition (MOCVD) [12], electro-deposition [13], vapor–liquid–solid (VLS) epitaxy [14], pulsed laser deposition (PLD) [15] and template-based methods [16, 17]. Recently, growth of aligned ZnO nanorods/nanowires using a hydrothermal method in aqueous solution at low temperatures (<100°C) was reported [18]. The aqueous-solution method is a simple-facility, no-catalyst and low-cost process and is adaptable to fabricate large-area ZnO nanorods with good uniformity at low temperatures [19–21].

Before the growth of well-aligned ZnO nanorods by the aqueous-solution method, a seed layer is usually coated on the substrate, and then vertically aligned ZnO nanorods are grown using the hydrothermal aqueous-solution process [18, 20, 22, 23]. There are many kinds of seed layers reported, such as spin-coated ZnO seed nanoparticles [19], sol–gel seed layers [23] and RF magnetron sputtered ZnO-based seed layers [24]. It has been found that the properties of the ZnO nanorods have a dependence on the pre-treatment condition of the seed layer by sol–gel. And, the annealing of the seed layer before the nanorod growth, i.e. pre-annealing, has a significant influence on the nanorod growth [22]. In comparison with a sol–gel seed layer, the sputtered ZnO seed layer has some advantages, such as easy thickness control, good morphology and process repeatability. So, in this study, ZnO nanorods formed by hydrothermal growth on

S.-Y. Liu · T. Chen · J. Wan · G.-P. Ru · B.-Z. Li · X.-P. Qu (✉)
State Key Laboratory of ASIC and System, Department of Microelectronics, Fudan University, Shanghai 200433, China
e-mail: xpqu@fudan.edu.cn
Fax: +86-21-65643768

Table 1 The annealing temperature of the seed layers, the density, the average length and the typical diameters of the corresponding ZnO nanorods

Annealing temperature of the seed layers (°C)	Density of ZnO nanorods (rods cm^{-2})	Average length of ZnO nanorods (nm)	Typical diameter of ZnO nanorods (nm)
Room temperature	2.56×10^{10}	262.3	43
200°C	2.40×10^{10}	300.2	46
400°C	1.54×10^{10}	404.7	52
600°C	1.50×10^{10}	501.6	60

ion-beam-sputtered ZnO seed layers pre-annealed at different temperatures were systematically investigated. Our work demonstrates that the crystallinity, growth rate and optical properties of the ZnO nanorods strongly depend on the pre-treatment of the seed layers.

2 Experimental

Si wafers covered with 500-nm SiO_2 were used as substrates. After a standard chemical cleaning, the substrates were loaded into an Oxford sputtering system. Then, the ZnO seed layers were deposited by an ion beam sputtering technique using a ceramic ZnO target (99.99% purity) at room temperature. The base pressure was about 9×10^{-5} Pa and the working Ar pressure was 5×10^{-3} Pa. After deposition, the samples were immediately annealed at temperatures from 200 to 600°C in air ambient for 15 min. The highest annealing temperature of 600°C was chosen because of its compatibility with the process using glass as substrate.

ZnO nanorods were then grown on the ZnO seed layer by a hydrothermal approach. Equal molar aqueous solutions of zinc nitrate hexahydrate ($Zn(NO_3)_2 \cdot 6H_2O$, 0.01 M) and hexamethylenetetramine ($C_6H_{12}N_4$, 0.01 M) were mixed in a pyrex glass bottle. The substrates were placed in a Teflon boat to keep them upright in the bottle. Then, the sealed glass bottle was put into a laboratory oven and heated to 75°C for 5 h. Finally, the samples were rinsed in flowing deionized water immediately after taking out of the solution to remove any residual salt on the surface and then were dried in N_2 at room temperature (RT).

The structure and morphology of the ZnO nanorods were characterized by X-ray diffraction (XRD) using monochromatic Cu Kα radiation ($\lambda = 1.54$ Å) and field emission scanning electron microscopy (SEM). The atomic concentration ratio was measured by Kratos AXIS $Ultra^{DLD}$ X-ray photoelectron (XPS) spectroscopy. The optical property of the ZnO nanorods was measured by photoluminescence (PL) spectroscopy using the 325-nm beam of a He–Cd laser at room temperature.

3 Results and discussion

Figures 1a–d show the top-view SEM images and the cross-sectional ones (insets) of the ZnO nanorods grown on the ZnO seed layers annealed at different temperatures, which are: as-deposited (room temperature), 200, 400 and 600°C, respectively. All the nanorods were grown at 75°C for 5 h. It can be seen that the obtained ZnO nanorods were vertically oriented with respect to the substrates and at the top end seemed a little tilted. Table 1 lists the density, the average length and the typical diameters of the corresponding ZnO nanorods on the seed layers annealed at different temperatures. The density of the ZnO nanorods decreases with increase of the pre-annealing temperature of the seed layers, from 2.56×10^{10} and 2.40×10^{10} cm^{-2} to 1.54×10^{10} and 1.50×10^{10} cm^{-2}, corresponding to the pre-annealing temperatures from RT and 200 to 400 and 600°C, respectively. Seen from the cross-sectional SEM images, the average lengths of the ZnO nanorods were higher with the increasing annealing temperature of the seed layer, in the order of: room temperature (∼262 nm) < 200°C (∼300 nm) < 400°C (∼404 nm) < 600°C (∼501 nm). This result demonstrates that the growth rate of ZnO nanorods has a strong dependence on the seed layers. The typical diameters of the ZnO nanorods gradually increased from 40 to 60 nm with the increasing annealing temperatures of the seed layer. Compared to change of the length, the diameters of the ZnO nanorods were not strongly influenced by the seed layer annealing temperatures.

In order to explore the effect of seed layers on the ZnO nanorod growth, the morphologies of the sputtered ZnO seed layers annealed at different temperatures were observed by SEM, as shown in Fig. 1e–h. The grain size of the seed layers was enhanced with the increasing seed layer annealing temperature, indicating improved crystallinity of the seed layer. It was reported that the diameters of the ZnO nanorods depended on the particle size of the seed layer [20, 24]. In our study, the diameters of the nanorods were also increased with the increase of the pre-annealing temperature of the seed layers, which may be due to the enhancement of the grain size of the seed layers. The pre-annealing treatment would integrate small grains to form larger ones,

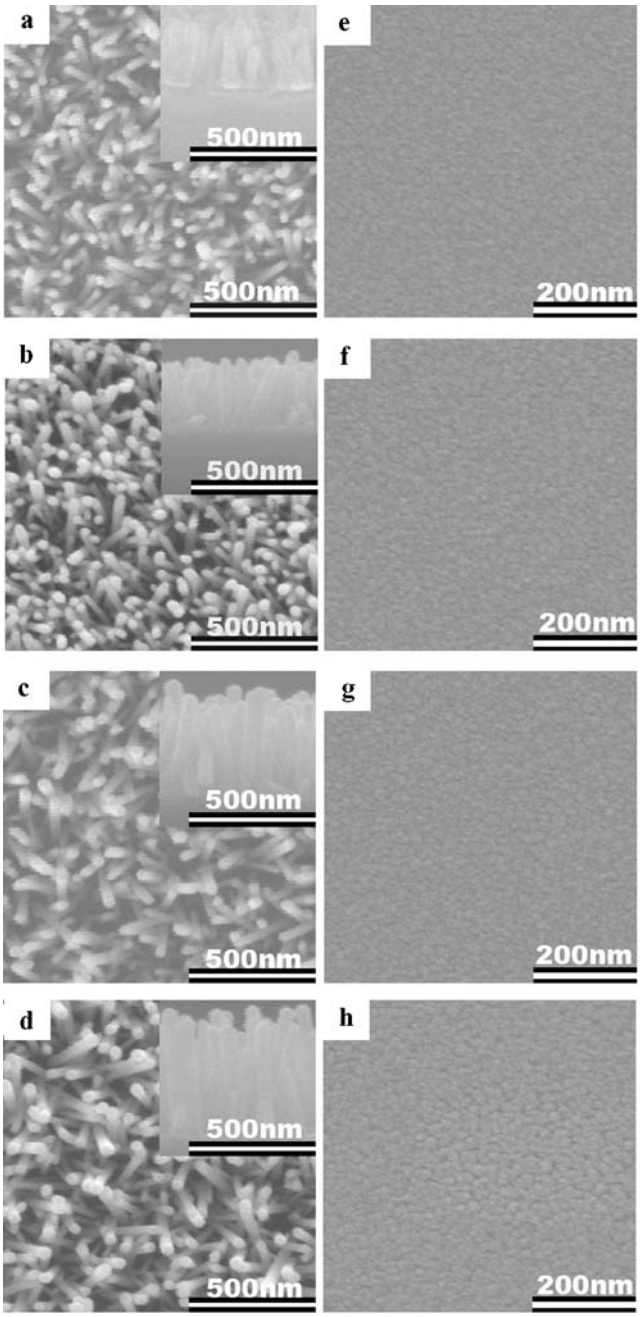

Fig. 1 The SEM images of the top view and cross section (*inset*) of ZnO nanorods grown from the seed layers annealed at different temperatures: **a** room temperature, **b** 200°C, **c** 400°C and **d** 600°C and the images of the corresponding ZnO seed layers annealed at different temperatures: **e**, **f**, **g** and **h**

which will reduce the number of the particles, corresponding to the decreasing number of the nucleation sites of ZnO nanorods thereon. This can explain the phenomenon that the density of the nanorods decreases with the increasing seed layer annealing temperatures.

XRD was further used to characterize the crystallinity of the seed layers annealed at different temperatures. In Fig. 2,

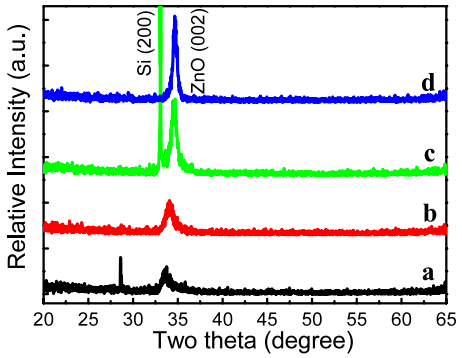

Fig. 2 XRD patterns of the sputtered ZnO seed layers annealed at various temperatures: **a** room temperature, **b** 200°C, **c** 400°C and **d** 600°C

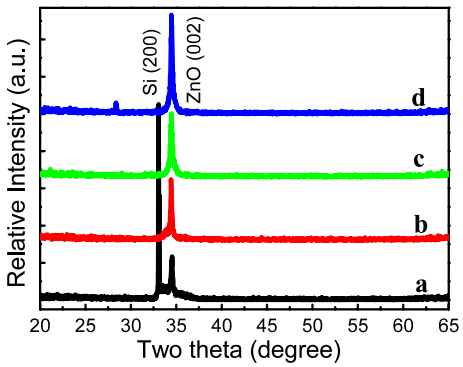

Fig. 3 XRD patterns of the corresponding ZnO nanorods of ZnO seed layers annealed at various temperatures: **a** room temperature, **b** 200°C, **c** 400°C and **d** 600°C

curve (a) shows that the as-deposited ZnO film has a broad diffraction peak, indicating an amorphous or nanocrystalline structure. The annealed ZnO films have a preferential orientation along the (002) plane. The increased (002) peak intensity and decreased full width at half maximum (FWHM) of the annealed ZnO seed layers with the increase of the annealing temperature indicate that the crystallinity of the film is effectively improved by supplying sufficient thermal energy of the annealing process.

Figures 3a–d show the XRD patterns of the ZnO nanorod arrays, corresponding to the SEM images shown in Fig. 1a–d. The indexed diffraction peaks are consistent with the standard values of the bulk ZnO crystal (JCPDS 36-1451) and show that all the ZnO nanorods have a wurtzite structure. The sharp and strong ZnO(002) peak indicates that the ZnO nanorods have a preferential *c*-axis orientation on sputtered ZnO seed layers [25]. The (002) d values ($d = 2.60$ Å) of the ZnO nanorods are nearly equal to that of the bulk ZnO and did not change much with the pre-annealing temperature of the seed layer. In the XRD patterns of ZnO nanorods, we did not observe the (100) and (101) peaks, while these peaks can be found in some samples grown on the sol–gel seed layers [22, 23]. The intensity of the (002) diffraction

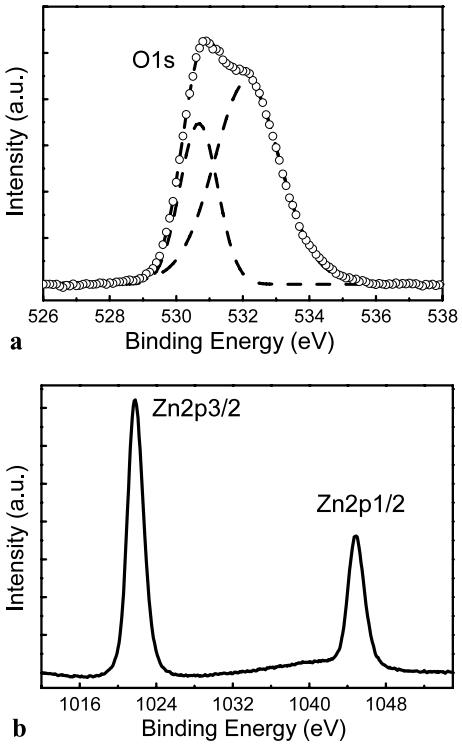

Fig. 4 X-ray photoemission spectroscopy (XPS) spectra of the obtained ZnO nanorods with seed layer pre-annealed at 600°C. **a** O 1s peak (*circle*: experimental data; *dashed lines*: fitting curves) and **b** Zn 2p3/2 and Zn 2p1/2 peaks

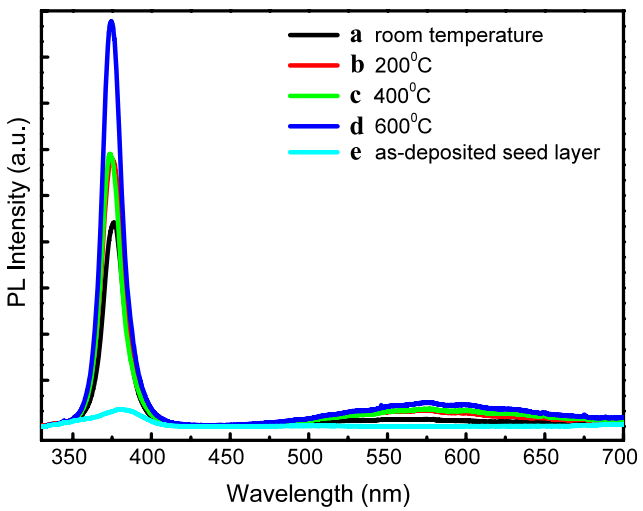

Fig. 5 Room-temperature PL spectra of the ZnO nanorods of ZnO seed layers with different annealing temperatures: **a** room temperature, **b** 200°C, **c** 400°C, **d** 600°C and **e** as-deposited ZnO seed layer

peak increases with the increase of the seed-layer annealing temperature, which can be attributed to the better alignment and the increasing length of the ZnO nanorods, as seen in Fig. 1.

Although the mechanism for the influence of the seed layer on the growth of ZnO nanorods thereon is still not very clear, the experimental results always demonstrate that usually the ZnO nanorods with the seed layer having the strongest [0001] orientation will have the highest growth rate. The nanorod arrays grow along the [0001] direction, due to the final obtained product with lowest surface free energy [24, 25]. In our study, we also observed this phenomenon. The pre-annealing improved the crystallinity of the seed layer and the growth rate of the obtained ZnO nanorods increases with the increase of the pre-annealing temperature. The crystal structure of ZnO can be presented by a number of alternating planes composed of coordinated Zn and oxygen atoms along the *c*-axis. Usually, the top surface is Zn-terminated [0001] while the bottom surfaces are O-terminated [000$\bar{1}$], resulting in a normal dipole moment and a polar surface [25]. In the hydrothermal reaction, the polar ZnO surface would attract opposite charges (Zn^{2+}) or (OH^{-}) from the solution, and form ZnO nuclei. In our case, the increased pre-annealing temperature for the seed layer may improve the reactivity of the seed-layer surface and results in a stronger electrostatic interaction between the polar surface and the ZnO nuclei in the solution [26]. Thus, more ZnO nuclei will be attracted on the seed layer annealed at higher temperature and result in a higher growth rate.

Figures 4a and b show the O 1s and Zn 2p X-ray photoemission spectroscopy (XPS) spectra of the obtained ZnO nanorods with the seed layer pre-annealed at 600°C. Only C 1s, O 1s, Zn 2p3/2 and Zn 2p1/2 signals were observed in the full spectrum and no peaks from other impurity elements were found. Figure 4a shows that there are two peaks centered at 530.68 and 532.13 eV. The peak located at 530.68 eV corresponds to the O^{2-} ions from the wurtzite structure of ZnO crystal [27], while the peak at 532.13 eV is attributed to the adsorbed H_2O or O_2 [28]. Since the sample was stored in air for several days and without Ar etching during measurement, the oxygen content from the absorbed H_2O or O_2 counted for a large part of the whole oxygen content. From Fig. 4a and b we find that the atomic concentration ratio of the O component (peak at 530.68 eV) of the wurtzite structure and the Zn component of the Zn 2p3/2 was non-stoichiometric and O deficient.

Figure 5 gives the room-temperature photoluminescence (PL) spectra of the ZnO nanorods grown on the seed layers annealed at different temperatures. In comparison, the PL spectrum of the as-deposited ZnO seed layer is also shown in Fig. 5e. For the as-deposited ZnO seed layer, there is a wide weak ultraviolet band-edge emission peak centered at 380 nm (3.26 eV) while, for the ZnO nanorod samples, sharper UV peaks located in the range of 374–377 nm were observed, indicating that the UV peak position of the ZnO nanorods is slightly shifted to shorter wavelength, i.e. a blue shift, which may be due to the size effect [29, 30]. The UV peak position and FWHM values for the samples are summarized in Table 2. Comparing the UV emissions of the

Table 2 The annealing temperature of the seed layers, UV peak position and FWHM of UV-PL peaks of the corresponding ZnO nanorods

Annealing temperature of the seed layers (°C)	Position of the UV peak (nm)	FWHM of the UV spectra (meV)
Room temperature	376.2	144.9
200°C	375.4	152.3
400°C	374.3	132.8
600°C	374.9	128.3

ZnO seed layer with the FWHM of 295 meV (Fig. 5e) and ZnO nanorod arrays thereon with the FWHM of 144.9 meV (Fig. 5a), we can see that the latter with a much sharper and higher peak effectively improve the UV optical properties. With the increase of the pre-annealing temperature, the intensity of the UV peak increases and the FWHM values (Table 2) of UV peaks of the ZnO nanorods are decreased from 144.9 to 128.3 meV for the nanorod sample with the annealing temperature of the seed layer increasing to 600°C. This demonstrates that the pre-annealing of the seed layer at higher temperature can obtain better-quality UV emission for the nanorods. Combining these results with the SEM results, we also find that the UV emission has a dependence on the alignment and the length of the nanorods, which is consistent with the XRD results.

From Fig. 5 we also observe a weak defect-related yellow–green emission band centered at ~577 nm (2.15 eV), which is commonly observed in hydrothermally grown ZnO nanorods [31, 32]. It shows the presence of a relatively low defect concentration in the ZnO nanorods in our experiments. Yellow emission has been attributed to oxygen interstitial defects (O_i) [33, 34]. More reports have attributed the yellow–green emission to the presence of OH groups [35–37] and our XPS also revealed the presence of a large amount of adsorbed OH groups. In addition, the intensity of the yellow–green emission increased with the increase of the pre-annealing temperature, reflecting an increasing concentration of the defects. The growth rate and length of the ZnO nanorods increase with the increasing of the pre-annealing temperature in this study, which may induce more lattice and surface defects and more adsorbed OH groups, leading to higher visible emission. This needs further investigation.

4 Conclusion

In this work, the pre-annealing effect of ion-beam-sputtered ZnO seed layers on the growth rate, density, crystallinity and optical properties of ZnO nanorods prepared by the hydrothermal method is studied. The ZnO nanorods obtained by the hydrothermal method grow dominantly in wurtzite structure and have a preferential (002) orientation with a vertical direction to the substrates. Our work demonstrates that the annealing treatment of the ZnO sputtered seed layer has an important influence on the crystallinity of the ZnO seed layer and the growth rate of the corresponding ZnO nanorods. As the annealing temperature increases, the preferred (001) orientation of the ZnO seed layer increases; the average length of the resulting ZnO nanorods increases from 262.3 to 501.6 nm and the density of the ZnO nanorods decreases from 2.56×10^{10} to 1.50×10^{10} cm^{-2}. XPS results show that the O and Zn ions in the wurtzite structure of the as-obtained ZnO nanorods are non-stoichiometric and O deficient. The PL spectra show strong UV emission peaks, with narrower FWHM with the increase of the pre-annealing temperature. It can be concluded that a higher pre-annealing temperature can improve the crystal quality of the ZnO seed layer and have a positive effect to improve the growth rate and the optical properties of the corresponding ZnO nanorods.

Acknowledgements This research is partly supported by the Shanghai Municipal Science and Technology program (08QH14002) and the National Key Basic Research program (2006CB302703). The authors greatly acknowledge support from the Micro and Nano Electronic Innovation Platform.

References

1. K. Nakahara, H. Takasu, P. Fons, A. Yamada, K. Iwata, K. Matsubara, R. Hunger, S. Niki, Appl. Phys. Lett. **79**, 4139 (2001)
2. Z.K. Tang, G.K.L. Wong, P. Yu, M. Kawasaki, A. Ohtomo, H. Koinuma, Y. Segawa, Appl. Phys. Lett. **72**, 3270 (1998)
3. U. Ozgur, Y.I. Alivov, C. Liu, A. Teke, M.A. Reshchikov, S. Dogan, V. Avrutin, S.J. Cho, H. Morko, J. Appl. Phys. **98**, 041301 (2005)
4. D.M. Bagnall, Y.F. Chen, Z. Zhu, T. Yao, S. Koyama, M.Y. Shen, T. Goto, Appl. Phys. Lett. **70**, 2230 (1997)
5. Y.W. Heo, D.P. Norton, L.C. Tien, Y. Kwon, B.S. Kang, F. Ren, S.J. Pearton, J.R. LaRoche, Mater. Sci. Eng. R **47**, 1 (2004)
6. M.H. Huang, S. Mao, H.Q. Feick, H.Q. Yan, Y.Y. Wu, H. Kind, E. Weber, R. Russo, P.D. Yang, Science **292**, 1897 (2001)
7. H. Rensmo, K. Keis, H. Lindstrolm, S. Soldergren, A. Solbrand, A. Hagfeldt, S.E. Lindquist, L.N. Wang, M. Muhammed, J. Phys. Chem. B **101**, 2598 (1997)
8. L. Liao, H.B. Lu, J.C. Li, C. Liu, D.J. Fu, Appl. Phys. Lett. **91**, 173110 (2007)
9. S. Liang, H. Sheng, Y. Liu, Z. Hio, Y. Lu, H. Shen, J. Cryst. Growth **225**, 110 (2001)
10. D.K. Hwang, S.H. Kang, J.H. Lim, E.G. Yang, J.Y. Oh, J.H. Yang, S.J. Park. Appl. Phys. Lett. **86**, 222101 (2005)
11. N.W. Emanetoglu, J. Zhu, Y. Chen, J. Zhong, Y.M. Chen, Y.C. Lu, Appl. Phys. Lett. **85**, 3702 (2004)
12. W.I. Park, G.C. Yi, Adv. Mater. **16**, 87 (2004)
13. J. Nayak, S.N. Sahu, J. Kasuya, S. Nozaki, J. Phys. D: Appl. Phys. **41**, 115303 (2008)
14. M. Huang, Y. Wu, H. Feick, N. Tran, E. Weber, P.D. Yang, Adv. Mater. **13**, 113 (2001)
15. J.H. Choi, H. Tabata, T. Kawai, J. Cryst. Growth **226**, 493 (2001)
16. T. Martensson, P. Carlberg, M. Borgstrom, L. Montelius, W. Seifert, L. Samuelson, Nano Lett. **4**, 699 (2004)

17. X. Wang, C.J. Summers, Z.L. Wang, Nano Lett. **4**, 423 (2004)
18. L. Vayssieres. Adv. Mater. **15**, 464 (2003)
19. M.H. Sun, Q.F. Zhang, J.L. Wu, J. Phys. D: Appl. Phys. **40**, 3798 (2007)
20. J.B. Cui, C.P. Daghlian, U.J. Gibson, R. Pusche, P. Geithner, L. Ley, J. Appl. Phys. **97**, 44315 (2005)
21. P.X. Gao, J.H. Song, J. Liu, Z.L. Wang, Adv. Mater. **19**, 67 (2003)
22. J.S. Huang, C.F. Lin, J. Appl. Phys. **103**, 014304 (2008)
23. T. Ma, M. Guo, M. Zhang, Y.J. Zhang, X.D. Wang, Nanotechnology **18**, 035605 (2007)
24. J.J. Song, S. Lim, J. Phys. Chem. C **111**, 596 (2007)
25. Z.L. Wang, J. Phys.: Condens. Matter **16**, R829 (2004)
26. A. Dev, S.K. Panda, S. Kar, S. Chakrabarti, S. Chaudhuri, J. Phys. Chem. B **110**, 14266 (2006)
27. X.Q. Wei, B.Y. Man, M. Liu, C.S. Xue, H.Z. Zhuang, C. Yang, Physica B **388**, 145 (2007)
28. M. Chen, X. Wang, Y.H. Yu, Z.L. Pei, X.D. Bai, C. Sun, R.F. Huang, L.S. Wen, Appl. Surf. Sci. **158**, 134 (2000)
29. P.C. Chang, C.J. Chien, D. Stichtenoth, C. Ronning, J.G. Lu, Appl. Phys. Lett. **90**, 113101 (2007)
30. Y.H. Yang, X.Y. Chen, Y. Feng, G.W. Yang, Nano Lett. **7**, 3879 (2007)
31. D. Li, Y.H. Leung, A.B. Djurisic, Z.T. Liu, M.H. Xie, S.L. Shi, S.J. Xu, W.K. Chan, Appl. Phys. Lett. **85**, 1601 (2004)
32. A.B. Djurisic, Y.H. Leung, K.H. Tam, L. Ding, W.K. Ge, H.Y. Chen, S. Gwo, Appl. Phys. Lett. **88**, 103107 (2006)
33. L.E. Greene, M. Law, J. Goldberger, F. Kim, J.C. Johnson, Y. Zhang, R. Saykally, P.D. Yang, Angew. Chem. Int. Ed. **42**, 3031 (2003)
34. X.L. Wu, G.G. Siu, C.L. Fu, H.C. Ong, Appl. Phys. Lett. **78**, 2285 (2001)
35. W.M. Kwok, A.B. Djurišić, Y.H. Leung, D. Li, K.H. Tam, D.L. Phillips, W.K. Chan, Appl. Phys. Lett. **89**, 183112 (2006)
36. N.S. Norberg, D.R. Gamelin, J. Phys. Chem. B **109**, 20810 (2005)
37. R. Xie, T. Sekiguchi, T. Ishigaki, N. Ohashi, D. Li, D. Yang, B. Liu, B.Y. Bando, Appl. Phys. Lett. **88**, 134103 (2006)